2014

Comprehensive Model of a Single-screw Expander for ORC-Systems

Davide Ziviani
Ghent University, Belgium, davide.ziviani@ugent.be

Ian Bell
University of Liege, ian.bell@ulg.ac.be

Martijn van den Broek
Ghent University, Belgium, Martijn.vandenBroek@UGent.be

Michel De Paepe
Ghent University, Belgium, michel.depaepe@ugent.be

Comprehensive Model of a Single Screw Expander for ORC-Systems

Davide ZIVIANI[1,2*], Ian BELL[3], Michel DE PAEPE[2], Martijn VAN DEN BROEK[1,2]

[1] Ghent University, Department of Industrial System and Product Design, Kortrijk, Belgium
davide.ziviani@ugent.be, martijn.vandenbroek@ugent.be

[2] Ghent University, Department of Flow, Heat, and Combustion Mechanics, Ghent, Belgium
michel.depaepe@ugent.be

[3] University of Liège, Thermodynamics Laboratory, Liège, Belgium
ian.bell@ulg.ac.be

* Corresponding Author

ABSTRACT

The Organic Rankine Cycle (ORC) system is considered one of the leading technologies for waste heat recovery applications. In order to increase the overall efficiency, design improvements and optimization analyses are necessary. The expander is the key component to convert the thermal energy in useful work. Several volumetric and turbine expanders have been investigated. Among volumetric machines, scroll, twin-screw and vane-type expanders are the main technologies. Recently, a number of experimental studies on single screw expanders (SSE) have been carried out, demonstrating the feasibility of employing such machine as an ORC expander. The single screw configuration presents a number of advantages over twin screw including balanced loading of the main screw, long working life, high volumetric efficiency. In this paper, a detailed geometry-based multi-chamber model of a single screw expander is presented. The model is based on a rotation-dependent function that entirely describes the geometry of the engaging surface between the screw rotor and the starwheels. The computation of the swept volume at each angular step and the inlet conditions, enables the solution of the system of differential equations governing the thermodynamic problem. The level of details of the model, which includes heat transfer losses, oil-flooded mixing and leakage paths calculation, allows the investigation of the impact of design changes to the expander machine performance. The validation of the proposed model is realized with experimental data obtained from an ORC set up which employs a SSE and Solkatherm (SES36) as working fluid. Test results have shown a maximum isentropic efficiency of 67% at 3000 rpm. The model predicts the mass flow rate and the power output within ± 10% and ± 15% respectively.

1. INTRODUCTION

Organic Rankine Cycle (ORC) systems represent a well proven technology to convert waste heat, ranging from high to low-grade heat (Quoilin et al., 2013). However, the optimization process of such systems is an open topic and covers different aspects such as working fluid selection, cycle architectures and components selection. In particular, the choice of the expander-type is crucial to optimize the power output.

Among volumetric machines, the single screw compressor (SSC), developed by Bernard Zimmern during the early 1960s (Zimmern and Patel, 1972), and well-established in the refrigeration industry, can be considered to be an improvement over twin-screw compressors because of balanced loading of the main screw, long working life, high volumetric efficiency, low leakage, low noise, low vibration and simplified configuration. Recently the SSC has begun to be investigated as a potential volumetric expander for ORC applications.

The aim of this paper is to develop and validate a detailed model of a single screw expander (SSE) based on geometric parameters and a set of differential equations. The proposed model is validated against experimental data.

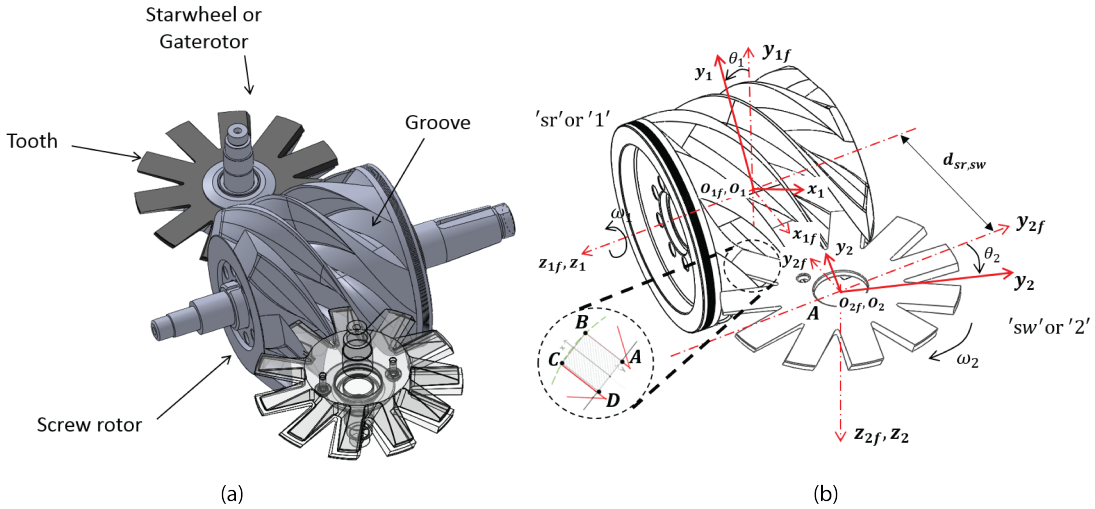

Figure 1: (a) 3D CAD model of single screw expander; (b) kinematics of the meshing pair.

2. SURVEY OF EXISTING SINGLE SCREW COMPRESSOR MODELS

The most common SSC configuration is the cylindrical-plate (CP), and includes as primary components a screw rotor and two starwheels or gaterotors, as shown in Figure 1a. The operating principle consists of a symmetric meshing between the screw rotor and the two starwheels. Due to this configuration, the total swept volume is divided in two equal parts which balances the loads. In fact, compared to other kinds of compressors, e.g. twin-screw type, the SSC has many advantages due to its symmetrical structure and well balanced radial gas pressure on the screw rotor. The simulation models available in literature are limited to single screw compressors. For instance, Bein and Hamilton (1982) developed a computer model of a low pressure oil-flooded single screw air compressor. An iterative method based on the polytropic coefficient was used to correlate internal predictions with empirical values. Leakage paths were also considered, neglecting the two-phase flow through the gaps. The heat transfer between the air in the compression chamber and oil was neglected. Boblitt and Moore (1984) presented a FORTRAN-based computer model of an oil-flooded single screw compressor operating at 100% capacity at matched discharge pressures, meaning the pressure at the end of the compression process corresponded exactly with the discharge pressure. The model is based on two empirical parameters, i.e. polytropic compression efficiency and the discharge flow coefficient. The included leakage model is based on the model proposed by Bein and Hamilton (1982), with the addition of the effects of the oil on the volumetric and isentropic efficiencies. Similarly, Wu and Jin (1988) developed a single screw compressor model including preheat, pressurization of the gas in the control volume during the suction and closure processes, flow of gas and oil mixture through the discharge port, leakage of gas and oil. Several effects, such as oil-injection rate, clearances and length of leakage paths, discharge port area variation, and oil shear power were included.

3. SINGLE SCREW EXPANDER GEOMETRY-BASED MODEL

In order to develop a geometry-based model, the analytic or numerical description of the meshing process has to be determined. As a consequence, the volume of the groove and its derivative with respect to rotation angle can be obtained. Furthermore, the geometric description allows the identification of the influence of the different leakage paths. Reference studies about the geometry can be found in literature concerning SSC, for example Chan et al. (1981), Hirai et al. (1986) and Sun (1988). Recently, the attention on SSE for ORCs is increasing. However, most of the research work is focused on experimental studies. Wang et al. (2011) evaluated the performances of a single screw expander prototype by using air as working fluid with a design inlet flow rate of 1.1 Nm^3/min. The experimental tests were carried out at different intake flow, different humidity, constant torque and constant rotational speed. The results show a maximum power output of 5 kW at 2850 rpm and maximum adiabatic efficiency of 59%. The relatively low adiabatic efficiency value was explained by the poor lubrication system and the use of dry air as the working fluid. Lu et al. (2013) investigated a single screw expander with 175 mm diameter rotor by using a compressed air refrigeration

system. The SSE was able to reach an adiabatic efficiency above 65% with a temperature drop of 70°C. He et al. (2013) analyzed the influence of the intake pressure on the performance of a single screw expander with 175 mm diameter rotor. The experimental results showed that high values of intake pressure negatively affect the power output. A resonance phenomenon occurred in the range 2000 rpm and 2200 rpm, leading to large leak rates. The maximum power output of 22 kW was obtained at 2800 rpm and the highest adiabatic efficiency was around 55%.

3.1 Generation of the Main Rotor

The generation of the rotor, with the support of a CAD software, requires the solution of the kinematics of the meshing between starwheel (*sw*) and screw rotor (*sr*). Due to the cylindrical-plate configuration of the SSE, the problem can be addressed by considering the double-enveloping worm gear theory (Litvin, 1994). Hence, the screw rotor is obtained by an envelope of a one-parameter family of starwheel surfaces. The considered SSE has 6 grooves in the main rotor and 11 teeth in the starwheels, which automatically defines the correlation between rotation angle and angular speed of the meshing pair:

$$i = \frac{z_{sw}}{z_{sr}} = \frac{\theta_{sr}}{\theta_{sw}} = \frac{\omega_{sr}}{\omega_{sw}}. \tag{1}$$

By considering a straight-line envelope meshing pair (SEMP or LEMP), fixed and movable coordinate systems have to be defined for both main rotor and starwheel. The right-handed reference systems are shown in Figure 1b. Furthermore, each starwheel tooth engages a groove with three sides, identified by segments $\overline{AB}$, $\overline{BC}$ and $\overline{CD}$. As a consequence, the solution of kinematics problem has to be guaranteed for each side of the generating tooth, as described by Yang (2002). The general position vector of a family of two parameters curves is given by

$$\mathbf{r}_{1j}(u,\theta_1) = \mathbf{M}_{1,1f}\mathbf{M}_{1f,2f}\mathbf{M}_{2f,2}\mathbf{r}_{2j}(u,\theta_1). \tag{2}$$

The general meshing equations expressing the relative contact between groove and tooth, i.e. the cross product between the normal vector to the contact surface, $\mathbf{N}_f^2$, and the relative relative velocity $\mathbf{V}_f^{(21)}$, is given by

$$\mathbf{N}_f^2 \cdot \mathbf{V}_f^{(21)} = \left(\frac{\partial \mathbf{r}_{1j}}{\partial u} \times \frac{\partial \mathbf{r}_{1j}}{\partial \theta}\right) \cdot \mathbf{V}_f^{(21)} = 0, \tag{3}$$

where $j = \overline{AB}, \overline{BC}, \overline{CD}$. Eq. (2) and (3) have to be satisfied simultaneously. In Figure 1a, the full 3D model of the main rotor engaged with the starwheels is shown as obtained with 3D CAD software. The 3D geometry is used to validate the geometric properties of SSE.

3.2 Calculation of the Swept Volume

The SSE operation can be divided into three phases, i.e. suction, closed expansion and discharge. The geometric description of the SSE involves a number of parameters and the definition of important angles, such as the beginning of suction, the closing angle at which the trapped gas begins to expand and the discharge angle. In Figure 2, a schematic representation of SSE in *Matlab* is proposed. The reference system (z, r), adopted to describe the SSE geometry, is centered on the crossing point between main rotor rotational axis and the perpendicular starwheel axis. Furthermore, a brief list of formulae is listed. Generally speaking, the design of a SSE relies on the selection of the main rotor diameter D_{sr}. In fact, it is possible to demonstrate that all the most important dimensions are correlated to the main rotor diameter. For instance, the starwheel radius R_{sw} is related to the main rotor radius by a design coefficient λ_d and the swept volume can be defined as a function of D_{sr}^3, Sun (1988). The swept volume is calculated by correlating the engaging tooth area into the corresponding groove and the tooth engaging angle. Generally, two approaches can be considered to obtain the engaging area, i.e. through an analytic function or a polygonal approach which requires the definition of four corner points of a tooth at each rotation angle. In this paper, the first approach is adopted during the closed expansion. The engaging angle of each tooth, defined as the angle between the first point of contact of the tooth with one flank of the groove until the tooth completely disengages the groove, is approximately $\alpha_{sw} = 90$ °, which corresponds to $\alpha_{sr} \approx 160$ °. The maximum groove volume is calculated as a sum of two contributions, $V_o = V_{g,1} + V_{g,2}$, related to geometry-defined angles. The first part represents the volume between suction angle and closing angle and the second part is the volume from closing angle to discharge angle. Normally, the maximum groove volume is associated with the discharge volume, i.e. $V_o = V_2$, which is related to the suction volume V_1 by means of the volumetric built-in ratio, fixed by design.

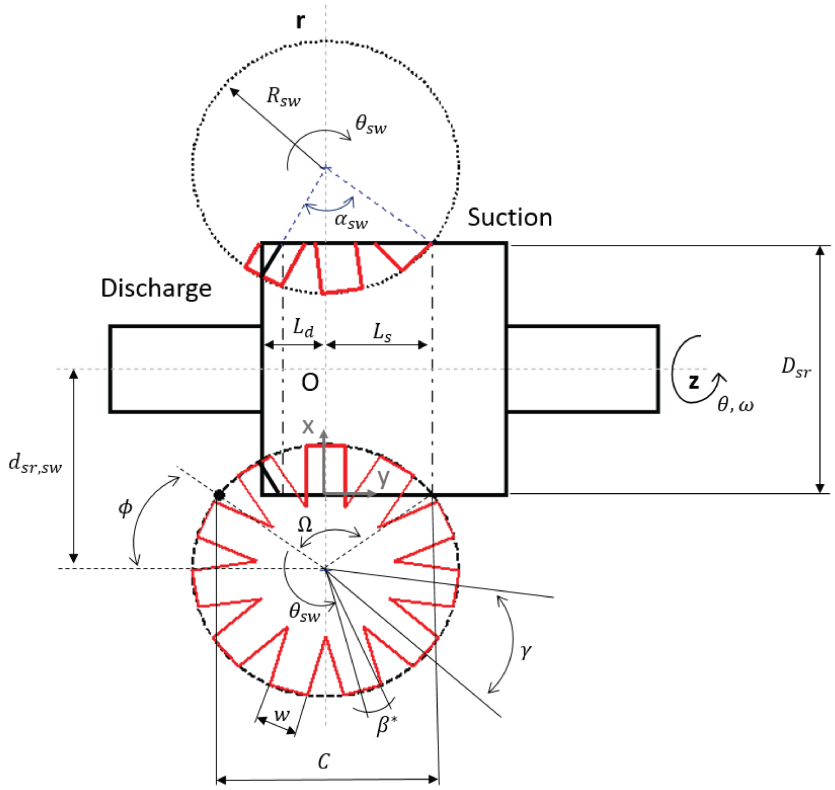

$r_{v,built-in} = V_2/V_1$
$D_{sr} = const$
$\alpha_{sw} = \pi/2$, $\alpha_{sr} = i\,\pi/2$
$R_{sw} = \lambda_d R_{sr}$, $\lambda_d = 1 to 1.1$
$\lambda_{opt} = f(\gamma, \lambda_d)$, according to Jin et al. (2006)
$d_{sr,sw} = \alpha_{opt} D_{sr}$
$w \approx 0.3\, R_{sr}$
In terms of starwheel rotation angle:
$\gamma = 2\pi/z_{sw}$
$\beta_s = \cos^{-1}\left(\frac{d_{sr,sw}-R_{sr}}{R_{sw}}\right)$
$\beta^* = \sin^{-1}\left(\frac{w}{2R_{sw}}\right)$
$\beta_d = -(\alpha_{sw} - \beta_s - \beta^*)$

$\phi = \sin^{-1}\left(\frac{2d_{sr,sw}-D_{sr}}{D_{sw}}\right) = const$
$\Omega = \pi - 2\phi = const$
$C = 2R_{sw}\sin(\Omega/2)$, Lundberg and Gianvall (1979)
$L_s = R_{sw}\sin\beta_s$
$L_d = R_{sw}\sin\beta_d$
$L_{eff} = L_s + L_d$

Figure 2: Single screw expander geometric relationships.

The volume of the groove at each starwheel angle (or equivalently main rotor angle) can be calculated by describing the engaging tooth surface with local reference system (x, y) on the tooth. The expression of the swept volume is given by splitting the contribution into $V_{g,1}(\theta_{sw})$ and $V_{g,2}(\theta_{sw})$:

$$V(\theta_{sw}) = \begin{cases} \frac{i}{2}\int_{\beta_s+\beta^*}^{\theta_{sw}}\int_{-w/2}^{B}\frac{1}{\cos\theta_{sw}}\left[R_{sr}^2 - \left(d_{sr,sw} - \sqrt{R_{sw}^2 - y^2}\cos\theta_{sw} + y\sin\theta_{sw}\right)^2\right]dy\,d\theta_{sw}, & \beta_s + \beta^* \le \theta_{sw} \le \beta_{close}, \\ V_o - \frac{i}{2}\int_{\theta_{sw}}^{\beta_d}\int_{-w/2}^{w/2}\frac{1}{\cos\theta_{sw}}\left[R_{sr}^2 - \left(d_{sr,sw} - \sqrt{R_{sw}^2 - y^2}\cos\theta_{sw} + y\sin\theta_{sw}\right)^2\right]dy\,d\theta_{sw}, & \beta_{close} < \theta_{sw} \le \beta_d, \end{cases} \tag{4}$$

where

$$B = R_{sw}\sin\left[\cos^{-1}\left(\frac{d_{sr,sw}-R_{sr}}{R_{sw}}\right) - \theta_{sw}\right]. \tag{5}$$

Because of the absence of an analytic solution, the volume of the groove is calculated numerically at fixed increments of the rotation angle and a high order polynomial function is used to interpolate the discrete values and to obtain a continuous function as well as to guarantee the continuity of its derivative, necessary to solve the system of differential equations (9-11). Finally, by recalling that the expansion process occurs symmetrically in both sides of the main rotor, the theoretical volumetric flow rate is defined as follows:

$$\dot{V}_{th} = 2z_{sr}V_1 n. \tag{6}$$

3.3 Suction, Discharge and Leakage Models

The flows associated with the processes of suction and discharge are assumed to be isentropic, corrected by a contraction flow coefficient and the area is calculated from the geometry model at each crank angle. Furthermore, the port areas have been expressed in terms of the main rotor diameter, which means that by changing the value of the main rotor diameter, automatically all the dimensions are adjusted. The suction and discharge areas as function of rotation angle

can be expressed as sine function multiplied by the maximum area. Similarly to SSC, in the SSE it is possible to define 9 main leakage paths, as outlined by Bein and Hamilton (1982):

L1 Starwheel tip
L2 Starwheel leading flank
L3 Starwheel leading flank blowhole
L4 Starwheel trailing flank
L5 Starwheel trailing flank blowhole
L6 Starwheel window
L7 Main rotor leading thread land
L8 Main rotor trailing thread land
L9 Main rotor suction end band

Among them, L1 to L5 are related to the contact lines between tooth and groove and the wear of the starwheel. In this model, it is assumed that the teeth have no wear and therefore there are no gaps, i.e. $\delta_{1-5} = 0$. L6 corresponds to the leakage path associated with the gap between the upper part of the tooth and the housing, as shown in Figure 3b. A minimum value of the gap δ_6 has to be guaranteed in order to enable the rotation of the starwheel. The flow through flow path L6 is assumed as isentropic flow through a nozzle. The leading and trailing thread of the main rotor, L7 and L8 respectively, are characterized by a length which varies from zero at the beginning of suction untill the approximately maximum value at the beginning of discharge, with a phase difference of $2\beta^*$. Despite the fact that the radial gaps δ_{7-8} can be assumed constant, as is clear from Figure 3c, the land between the trailing thread of one groove and the trailing thread of the consecutive groove is not constant throughout the rotation. In particular, the minimum land corresponds to minimum resistance criteria for the groove flank and the maximum land is determined by the helical shape of each groove milled from a cylindrical surface. L7 and L8 are treated as friction corrected isentropic compressible flow through a nozzle (Bell et al., 2013). Finally, L9, the end band of the groove, is related to the sealing between the end rotor surface and the wall. Due to lack of data, δ_9 is assumed zero.

3.4 Heat Transfer Model

During the expansion process inside the SSE, the heat transfer takes place. In this model the heat transfer between the expanding gas and the main rotor as well the heat transfer between the shell and the ambient are taken into account. According to Bilen et al. (2009), the heat transfer coefficient for an internally grooved tube with trapezoidal section can be calculated as

$$h_{groove} = \frac{\lambda_g}{L_{groove}} \left(0.014 Re^{0.893} Pr^{1/3}\right), \tag{7}$$

where L_{groove} represents the characteristic length of the groove section and λ_g is the thermal conductivity of the refrigerant gas. The gas velocity used to calculate the Reynolds number is approximated with the peripheral velocity of the rotating groove.

An overall thermal conductance characterizes the heat transfer between the SSE shell and the environment. The heat rate exchanged is given by

$$\dot{Q}_{amb} = UA_{amb} \left(T_{amb} - T_{lump}\right), \tag{8}$$

where T_{amb} is the ambient temperature and T_{lump} is a lumped value for the temperature which is determined by closing the overall energy balance.

3.5 Governing Equations and Thermodynamic Properties

Due to the 11/6 configuration, three teeth are constantly engaged with the main rotor. For this reason, the model proposed takes into account three grooves at the same time, i.e. "G1", "G2" and "G3", as shown in Figure 3a and 3d. It is assumed that the thermodynamic conditions in the grooves at the same phase angle are the same and the overall process is identical for both sides of the SSE. Pressure and temperature of the gas and oil are assumed homogeneous throughout the control volume (CV). Potential and kinetic energies of the gas and oil are neglected. Furthermore, two more fixed control volumes, *sw*1 and *sw*2, are considered to represent the chambers where the starwheels are installed and the volumes of these chambers are estimated from CAD considerations. For each CV, mass, energy and liquid fraction, i.e. oil fraction, conservation equations are applied and expressed as:

$$\frac{dm_{CV}}{d\theta} = \frac{1}{\omega} \sum_j \dot{m}_j, \tag{9}$$

$$\frac{dT}{d\theta} = \frac{1}{m_{CV} c_{v,m}} \left\{ -T \left(\frac{\partial p}{\partial T}\right)_v \left[\frac{dV}{d\theta} - v \frac{dm_{CV}}{d\theta}\right] - m_{cv}(u_l - u_g) \frac{dx_l}{d\theta} - h \frac{dm_{CV}}{d\theta} + \frac{\dot{Q}_{groove}}{\omega} + \frac{1}{\omega} \sum_j \dot{m}_j h \right\}, \tag{10}$$

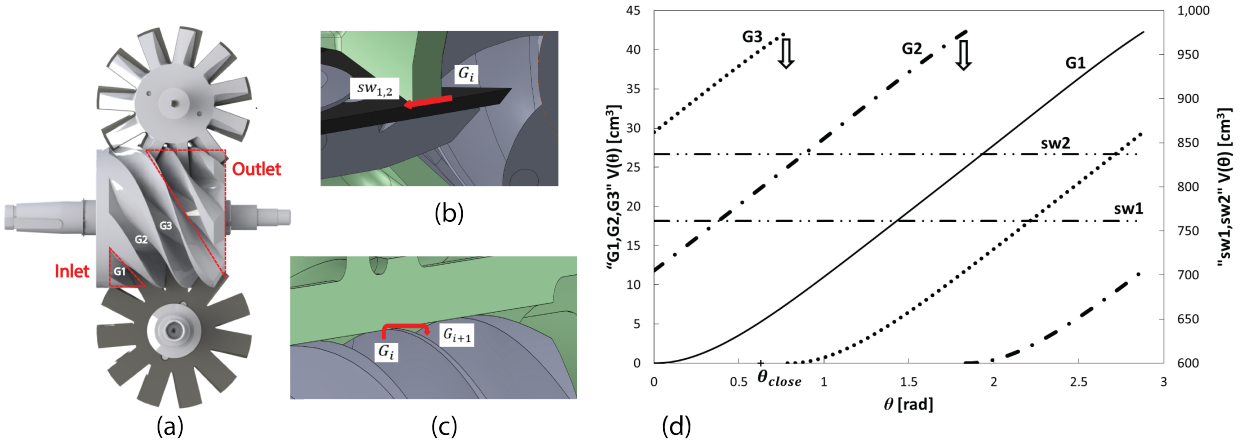

Figure 3: Single screw expander: (a) Control volumes; (b) Leakage paths; (c) $V(\theta)$ for each control volume during the engaging angle α_{sr}.

$$\frac{dx_l}{d\theta} = \frac{1}{m_{CV}}\left[\frac{1}{\omega}\sum_j \dot{m}_j x_{l,j} - x_l\frac{dm_{CV}}{d\theta}\right], \tag{11}$$

where the index *j* represents the number of flow paths coming in or going out of the CV.

The thermodynamic properties of the working fluid, i.e. Solkatherm, are retrieved by calling the CoolProp routines (Bell et al., 2014).

3.6 Solution Method

The overall model of the SSE has been implemented in the Python-based PDSim[1] library. The initialization of the simulation includes the specifications of the diameter of the main rotor and additional design parameters, along with the boundary conditions, i.e. inlet and outlet thermodynamic conditions. The program obtains the volume of the grooves as function of main rotor rotations and starts the iterative solution procedure. All the CVs are solved simultaneously. Because of the intrinsic and variable stiffness of the differential equations, an adaptive solver, namely RK45, is used to solve the system for each control volume . A specific function is introduced to handle the discontinuities of the volume function, as illustrated in Figure 3b. The convergence is ensured by specifying the minimum residual for the overall energy balance.

4. RESULTS AND DISCUSSION

4.1 Experimental Results

The SSE is installed in an ORC test system fed by thermal oil (Therminol 66). In Figure 4, it possible to observe part of the LabVIEW GUI used for the data acquisition and an inset highlighting the SSE. A more detailed description of the test-rig is given by Desideri *et al.* (2014). The main parameters of the expander are listed in Table 1, and the uncertainties of the installed sensors are specified in Table 2. It should be noted that some geometric parameters, such as rotor diameter, built-in volume ratio and swept volume have been estimated through the geometry model. The tests have been performed with SES36 as working fluid. The conditions at the expander inlet were maintained at saturated vapor or with a small degree of superheating ($\Delta T_{sh} \approx$ 5 to 10 K). The expander inlet pressure was varied in the range 3 to 7.5 bar at 100 to 125 °C. Instead the condensing pressure was maintained around 0.6 to 0.8 bar. The expander is connected to the grid through an inverter, which allows to modify the rotational speed of the expander. In this case, the expander rotational speed is kept fixed at 3000 rpm. In order to vary the refrigerant mass flow rate, the rotational speed of the multi-stage turbo pump has been adjusted in the range 1600 to 2000 rpm. Due to the fact that the oil in solution with the refrigerant in the entire ORC system is estimated to be around 3.23% of the total mass of fluid, the term x_l is considered zero. This approximation is also justified by the lack of accurate data of the amount of flooding inside the

[1] PDSim by I. Bell - pdsim.sourceforge.net

expander itself, which potentially plays a role in the leakages. A sample of operating conditions is listed in Table 3. The electrical power is calculated by introducing mechanical and electrical efficiency which affect the internal power of the expander:

$$\dot{W}_{el} = \eta_m \, \eta_{el} \, \dot{W}_{int}. \tag{12}$$

The power losses related to power transmitted from the expander to the generator by means of a shaft are associated to the mechanical efficiency and obtained by experiments. By analyzing the set of experimental data, it is possible to draw some considerations regarding the physical behavior of the SSE in the ORC system. In Figure 5, power output as a function of the expansion ratio is plotted for several operating points. Between expansion ratios 6 and almost 10, the power output is linear with the expansion ratio, in agreement with He et al. (2013). Around β_{exp} = 10, the isentropic efficiency of the expander drops because of the fixed built-in volume ratio, despite an increase in power output. Furthermore, in Fig. 5, a particular behavior of the expander for expansion ratios above 10 is also shown. In particular, the power output of the expander shows a flat behavior. In the current ORC system, the cold sink of the condenser is air-cooled and the temperature of the condenser cannot be controlled. The condensation pressure depends of the external ambient temperature. If the temperature of the hot source increases, since the air cooler usually is operated at its maximum capacity, the condensing pressure raises as a consequence. The explanation of the flat power output is related to the fact that while the inlet pressure of the expander is kept constant and therefore also the mass flow rate, a sudden change of external ambient conditions forces the condensing condition, in terms of pressure and temperature, to drop. Despite the decrease of the condensing pressure of about 0.2 bar, the power output is not influenced. For higher expansion ratios, the adiabatic efficiency decreases rapidly and in some cases, wet expansion was spotted, indicated by a sudden increase of the mass flow rate at fixed value of the expander inlet pressure. In Figure 6, a scattered contour plot of the isentropic efficiency at different expansion ratios is shown. As expected, the maximum value, ~66%, occurs around β_{exp} = 10. In some cases, higher values of the isentropic efficiency have been obtained, up to 67%.

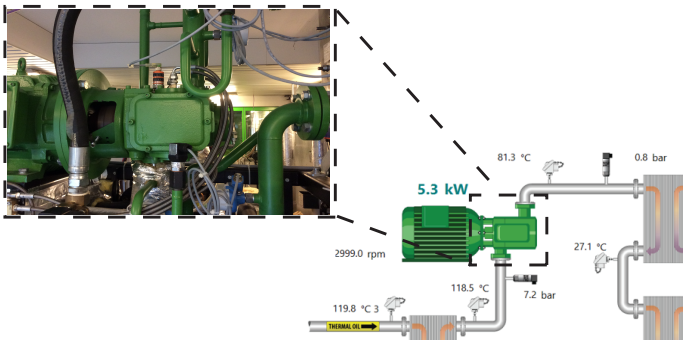

Figure 4: Snapshot of LabView control panel and the SSE installed in the ORC test-rig.

Parameters	
Engaging ratio	11/6
D_{sr} [m]	0.155
V_o [cm^3]	96
$r_{built-in}$ [-]	5
$\dot{W}_{nom}$ [kW]	11

Table 1: SSE geometric parameters.

Variable	Units	Uncertainty
T	°C	±0.18
p	bar	±0.016
$\dot{m}_{ORC}$	kg/s	0.1%
$\dot{W}_{el}$	W	0.1%

Table 2: Measured variables and their uncertainties.

4.2 SSE Model Validation

The model has been validated with the test results obtained. To achieve sufficient accuracy on the prediction of the performance of the SSE, the model has been first tuned by adjusting the flow coefficients of suction and discharge

Test Conditions	n [rpm]	$\dot{m}_{wf}$ [kg/s]	$T_{exp,in}$ [°C]	$p_{exp,in}$ [bar]	$T_{exp,out}$ [°C]	$p_{exp,out}$ [bar]	$\dot{W}_{el}$ [kW]	$\dot{W}_{p}$ [kW]
1	3001	0.191	97.2	3.354	76.5	0.583	1.463	0.3
2	2999	0.136	98.1	3.958	76.2	0.601	1.969	0.2
3	2999	0.130	99.9	4.53	76.8	0.625	2.662	0.2
4	2999	0.207	102.6	5.013	78.7	0.645	3.168	0.4
5	2999	0.187	111.4	5.648	84.7	0.692	3.74	0.2
6	2999	0.247	114.7	6.349	86.8	0.733	4.389	0.6
7	2999	0.228	123.8	7.166	91	0.77	5.28	0.7
8	2999	0.271	124.1	7.312	90.4	0.745	5.555	0.7
9	3000	0.272	124	7.293	90.2	0.724	5.654	0.7
10	2999	0.283	119.8	7.511	85.3	0.692	5.984	0.8

Table 3: SSE experimental operating conditions.

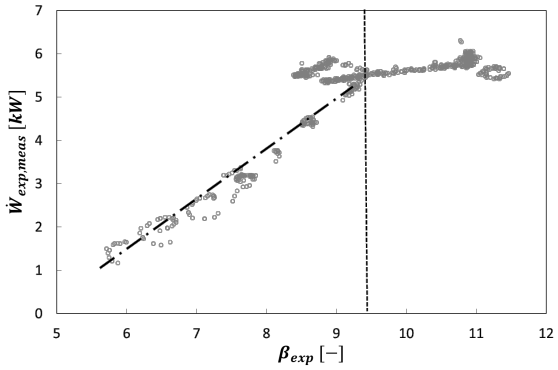

Figure 5: Experimental data of the expander power output as function of expansion ratios.

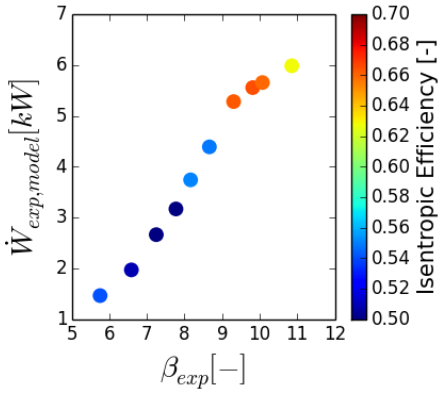

Figure 6: Isentropic efficency contour at different pressure ratio and power output.

ports, as well as the contraction coefficient of leakage paths. Generally, the flow coefficient is kept in the range 0.5 to 1. Besides the flow coefficients, another critical point of the model is the heat transfer analysis. Different heat transfer mechanisms occur during the entire expansion process from suction until discharge. In the majority of the cases, the discharge temperature is over-predicted by +15°C. One reason is related to the fact that the heat transfer during the inlet and filling processes have not been considered, in first instance. The second reason regards the heat transfer correlation adopted to model the in-groove heat transfer process. The correlation, adopted from internally grooved pipes, may underestimate the heat transfer rate. Further investigation has to be carried out to assess the heat transfer model. Due to the fact that assumptions have been made regarding the leakage paths, the calculated mass flow rate resulted to be over-predicted in all the cases. However, the spread of the calculated values and the measured ones is within ± 10%, as shown in Figure 7. Furthermore, the leakages play an important role in the overall performances. The mass flow rate through L8 resulted to be the most significant. As a consequence of the over-prediction of the mass flow rate, the power output is over-estimated up to 15%. In order to improve the agreement between calculated and measured values, the power losses have to be properly tuned. As a final conclusion, the model predicts the SSE performance within acceptable uncertainty. However, additional tuning and parametric analysis are needed to improve the accuracy especially regarding heat transfer mechanism and leakages.

5. CONCLUSIONS

A comprehensive simulation model for a novel single screw expander is proposed in this paper. A geometric model has been established in order to reproduce with high fidelity the meshing conditions between main rotor and starwheels.

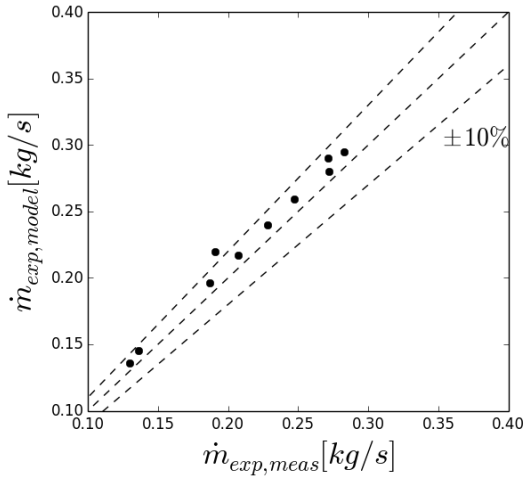

Figure 7: Comparison between calculated and measured mass flow rates.

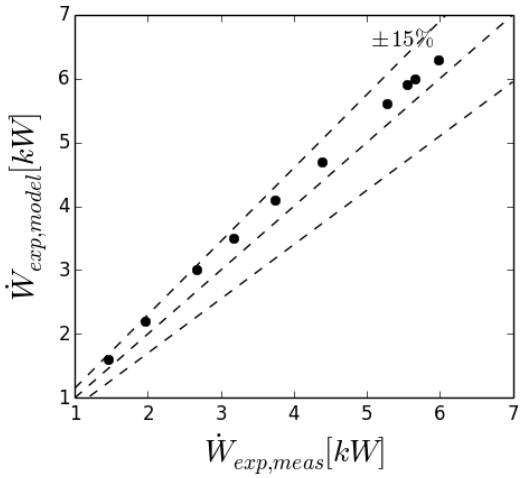

Figure 8: Comparison between calculated and measured power output.

The agreement of the model with experimental results is within 10% and 15% for the mass flow rate and power output, respectively. Further investigation on the effects of leakages and heat transfer has the potential to improve the predictions of the model.

NOMENCLATURE

Variable	Definition	Units
C	Distance	(m)
D	Diameter	(m)
h	Specific Enthalpy	(kJ/kg)
	Heat Transfer Coefficient	(kW/m^2K)
i	Transmission Ratio	(-)
L	Length	(m)
m	Mass	(kg)
$\dot{m}$	Mass Flow Rate	(kg/s)
M	Rotation Matrix	(-)
N	Normal Vector	(-)
p	Pressure	(kPa)
Pr	Prandtl Number	(-)
$\dot{Q}$	Heat Rate	(kW)
r	Position Vector	(m)
Re	Reynolds Number	(-)
T	Temperature	(K)
u	Specific Internal Energy	(kJ/kg)
UA_{amb}	Overall heat transfer conductance with ambient	(kW/K)
v	Specific Volume	(m^3/kg)
V	Volume	(m^3)
$\dot{V}$	Volumetric Flow Rate	(m^3/s)
V	Velocity Vector	(m/s)
w	Tooth width	(m)
z	Number of Grooves or Teeth	(–)
α	Angle	(rad)
β	Angle	(rad)
	Expansion Ratio	(-)

Variable	Definition	Units
δ	Clearance	(m)
λ	Thermal Conductivity	$(kW/m-K)$
θ	Rotation Angle	(rad)
ω	Angular Speed	(rad/s)
Ω	Angle	(rad)

Subscript	
amb	ambient
CV	Control Volume
exp	expander
el	electric
d	discharge
eff	effective
f	fixed
g	gas
int	internal
is	isentropic
l	liquid
m	mechanical
meas	measured
nom	nominal
p	pump
s	suction
sr	screw rotor
sw	starwheel
th	theoretical
v	volume
wf	working fluid

REFERENCES

Bein, T. W. and Hamilton, J. F. (1982). Computer modeling of an oil flooded single screw air compressor. In *International Compressor Engineering Conference*. Paper 383.

Bell, I. H., Groll, E. A., Braun, J. E., and Horton, W. T. (2013). A computationally efficient hybrid leakage model for positive displacement compressors and expanders. *Int. J. Refrigeration*, 36:1965--1973.

Bell, I. H., Wronski, J., Sylvain, Q., and Lemort (2014). Pseudo-pure fluid thermophysial property evaluation and the open-source thermophysical property library coolprop. *Ind. Eng. Chem. Res.*, 53:2498--2508.

Bilen, K., Cetin, M., Gul, H., and Balta, T. (2009). The investigation of groove geometry effect on heat transfer for internally grooved tubes. *Applied Thermal Engineering*, 29:753--761.

Boblitt, W. W. and Moore, J. (1984). Computer modeling of single-screw oil flooded refrigerant compressors. In *International Compressor Engineering Conference*. Paper 506.

Chan, C. Y., Haselden, G. G., and Hundy, G. (1981). The hallscrew compressor for refrigeration and heat pump duties. *Int. J. Refrigeration*, 4:275--280.

Desideri, A., van den Broek, M., Gusev, S., and Quoilin, S. (2014). Experimental campaign and modeling of a low-capacity waste heat recovery system based on a single screw expander. In *International Compressor Engineering Conference*. Paper 451.

He, W., Wu, Y., Peng, Y., Zhang, Y., Ma, C., and Ma., G. (2013). Influence of intake pressure on the performance of single screw expander working with compressed air. *Applied Thermal Engineering*, 51:662 □ 669.

Hirai, T., Noda, S., Sagara, Y., and Tsuzi, K. (1986). Performance analysis of oif single screw compressor. In *International Compressor Engineering Conference*. Paper 520.

Jin, G., Zhang, S., and Yu, X. (2006). Theoretical analysis of diameter ratio of engagement pair for singe screw compressor. In *International Compressor Engineering Conference*. Paper 1831.

Litvin, F. L. (1994). *Gear Geometry and Applied Theory*. Prentice-Hall, New Jersey.

Lu, Y., He, W., Wu, Y., Ji, W., Ma, C., and Guo, H. (2013). Performance study on the compressed air refrigeration system based on single screw expander. *Energy*, 55:762--768.

Lundberg, A. and Gianvall, R. (1979). A comparison of srm and globoid type screw compressors. *Int. J. Refrigeration*, 2:221--232.

Quoilin, S., Van Den Broek, M., Declaye, S., Dewallei, P., and Lemort, V. (2013). Techno-economic survey of organic rankine cycle (orc) systems. *Renewable and Sustainabe Energy Reviews*, 22:168--186.

Sun, G. (1988). The investigation of some basic geometric problems of the single screw co. In *International Compressor Engineering Conference*. Paper 630.

Wang, W., Wu, Y.T.and Ma, C., Liu, L., and Yu, J. (2011). Preliminary experimental study of single screw expander prototype. *Applied Thermal Engineering*, 31:3684 □ 3688.

Wu, J. and Jin, G. (1988). The computer simulation of oil-flooded single screw compressors. In *International Compressor Engineering Conference*. Paper 646.

Yang, S.-C. (2002). A mathematical model of the rotor profile of the single-screw compressor. *Proceedings of IMechE, Part C: J. of Mechanical Engineering Science*, 216:343--351.

Zimmern, B. and Patel, G. C. (1972). Design and operating characteristics of the zimmern single screw compressor. In *International Compressor Engineering Conference*. Paper 16.

ACKNOWLEDGEMENT

The results presented in this paper have been obtained within the frame of the IWT-130468 project. Additional acknowledgement goes to BEP Europe.